analytical chemistry

Article

pubs.acs.org/ac

Liquid Nebulization–Ion Mobility Spectrometry Based Quantification of Nanoparticle–Protein Conjugate Formation

Seongho Jeon,[†] Derek R. Oberreit,[‡] Gary Van Schooneveld,[§] and Christopher J. Hogan, Jr.*[,†]

[†]Department of Mechanical Engineering, University of Minnesota, Minneapolis, Minnesota 55455, United States

[‡]Kanomax-FMT, St. Paul, Minnesota 55110, United States

[§]CT Associates, Inc., Eden Prairie, Minnesota 55344, United States

Supporting Information

ABSTRACT: Despite the importance of examining the formation of nanoparticle–protein conjugates, there is a dearth of routine techniques for nanoparticle–protein conjugate characterization. The most prominent change to a nanoparticle population upon conjugate formation is a shift in the nanoparticle size distribution function. However, commonly employed dynamic light scattering based approaches for size distribution characterization are ineffective for non-monodisperse samples, and further they are relatively insensitive to size shifts of only several nanometers, which are common during conjugate formation. Conversely, gas phase ion mobility spectrometry (IMS) techniques can be used to reliably examine polydisperse samples, and are sensitive to ∼1 nm size distribution function shifts; the challenge with IMS is to convert nanoparticle–protein conjugates to aerosol particles without bringing about nonspecific aggregation or conjugate formation. Except in limited circumstances, electrospray based aerosolization has proven difficult to apply for this purpose. Here we show that via liquid nebulization (LN) with online, high-flow-rate dilution (with dilution factors up to 10 000) it is possible to aerosolize nanoparticle–protein conjugates, enabling IMS measurements of their conjugate size distribution functions. We specifically employ the LN-IMS system to examine bovine serum albumin binding to gold nanoparticles. Inferred maximum protein surface coverages (∼0.025 nm^{-2}) from measurements are shown to be in excellent agreement with reported values for gold from quartz crystal microbalance measurements. It is also shown that LN-IMS measurements can be used to detect size distribution function shifts on the order of 1 nm, even in circumstances where the size distribution function itself has a standard deviation of ∼5 nm. In total, the reported measurements suggest that LN-IMS is a potentially simple and robust technique for nanoparticle–protein conjugate characterization.

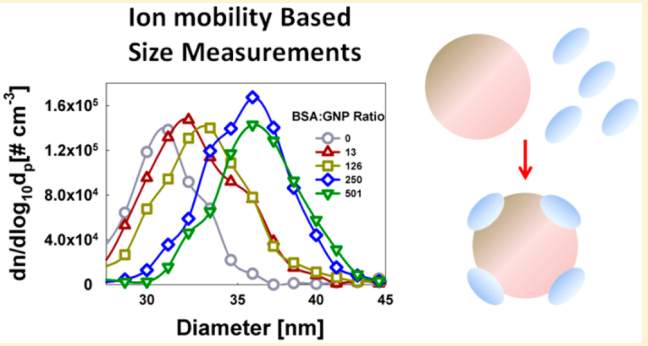

There is a need to develop and advance techniques to examine the extent of binding of proteins to nanomaterials/nanoparticles.[1−4] Within the bloodstream or other biological milieu, it is known that a protein corona will form on a nanoparticle's surface, altering its bioidentity and eventual fate.[5−9] At present, even in vitro with prescribed proteins and protein concentrations, binding is difficult to quantify; to date, no single technique is universally adopted for nanoparticle–protein conjugate quantification. The most notable change to an ensemble of nanoparticles upon protein binding is a shift of the nanoparticle size distribution function;[10] hence, it is the size distribution function that is most easily monitored to quantify binding. Size measurements of protein–nanoparticle conjugates have been carried out commonly with dynamic light scattering (DLS).[11−13] However, DLS is only applicable to highly monodisperse samples, with results skewed toward larger particles in polydisperse sample measurements. This is problematic for all but the most narrowly distributed particle size distributions. Polydisperse sample size distribution measurements can be better made via nanoparticle tracking analysis (NTA).[14−16] Unfortunately, NTA has limitations for particles/conjugates smaller than 30 nm in size; this prohibits direct examination of a number of nanoparticles as well as individual protein molecules. Further, both techniques are relatively unreliable in detecting small (less than ∼5 nm) size shifts, i.e., the data deconvolution schemes applied can lead to low measurement precision.

Techniques to examine protein–nanoparticle binding can be developed which are more precise than DLS and NTA. However, many of these techniques are limited to specific nanoparticle chemical compositions. For example, techniques relying on fluorescent labeling[1] or shifts in optical/plasmonic properties[17,18] of nanoparticles upon protein binding require specific particle optical properties. Liquid-phase size measure-

Received: April 20, 2016
Accepted: July 2, 2016

DOI: 10.1021/acs.analchem.6b01555
Anal. Chem. XXXX, XXX, XXX−XXX

ment techniques, such as asymmetric flow field fractionation[2,4] and analytical ultracentrifugation,[19] enable more rigorous quantification of size distribution functions, yet need to be coupled to appropriate detectors. Universal particle detectors for a variety of particle chemistries are not widely available.[20] Another alternative is gas-phase ion mobility spectrometry (IMS)[21] with a differential mobility analyzer (DMA),[22−24] which is a commonly employed technique for size distribution measurements of aerosol particles. In conjunction with condensation based single particle detectors,[25] DMAs facilitate size distribution function analysis in the 2−500-nm-diameter range, and unlike DLS and NTA, DMA data deconvolution schemes require minimal assumptions about the shape of the size distribution.[26] IMS is therefore more easily applied to polydisperse and multimodal samples,[27] and size shifts of several nanometers can be reliably detected.[28] The challenge in applying IMS to nanoparticle−protein conjugates is naturally that the conjugates must be introduced into the gas phase (aerosolized) without perturbing their size distribution functions. To date, aerosolization of liquid-phase samples has been accomplished almost exclusively with charge reduction electrosprays.[22,24,29] Notable demonstrations of the potential of IMS in nanoparticle−protein and nanoparticle−small molecule conjugate analysis have been carried out by Zachariah and co-workers,[28,30−34] with such charge reduction electrospray sources. Their measurements have consistently shown that by controlling the droplet size and concentration of analyte,[31] aerosolization with preservation of size distribution functions from the liquid phase is possible. In spite of this success, IMS has not been widely adopted in nanoparticle−protein conjugate size analysis. This is in large part because electrospray based aerosolization requires solutions/suspensions with electrical conductivities in a narrow range, as well as the a priori removal of nonvolatile solutes. These conditions are often mutually exclusive with the conditions needed to maintain nanoparticle stability in suspensions, i.e., the addition of salts and removal of surfactants lead to aggregation and settling of nanoparticles. As an example, noble metal nanoparticles and nanorods often need to be heat-treated post-electrospray to remove nonvolatile solute coating,[35,36] and such nanoparticles do aggregate and settle over the course of several days in electrosprayable (1−100 mM ammonium acetate) suspensions.[12]

Liquid nebulizers (LNs) have recently been developed with online, ultra-high-purity water dilution (by a factor of up to 10^4).[37] These LNs have number of advantages over both conventional nebulization/atomization techniques and electrosprays for application in hydrosol to aerosol conversion. Conventional nebulization technologies produce supermicrometer droplets, which, when dried, give rise to residue nanoparticles; residue particles mask the size distribution functions of the nanoparticles in suspension. Further, nonspecific aggregation, caused by the presence of multiple nanoparticles within a single droplet, is prevalent in conventional nebulization. By removing nearly all supermicrometer droplets via a ball impactor, and reducing the volume fraction of nonvolatile residue via online ultra-high-purity water dilution, nearly residue-free submicrometer droplets are produced with newer LNs. Nonspecific aggregation can also be predicted (with knowledge of the produced droplet size distribution) and mitigated via control over the extent of ultra-high-purity water dilution. In contrast with electrosprays, LN based aerosolization requires neither nonvolatile solute removal nor control of the suspension electrical conductivity. To date, such LN technology has enabled hydrosol to aerosol conversion with subsequent IMS measurements for nanoparticles as small as 5 nm,[37,38] and LN based aerosolization has proven capable of preserving nanoparticle size distributions for polydisperse and multimodal samples (where peaks differ by less than 5 nm).

The purpose of this study is to extend LN-IMS analysis for the first time to quantify bovine serum albumin binding to nominally 20, 30, and 50 nm gold nanoparticles (GNPs), demonstrating that this approach can be a simple and robust method for nanoparticle−protein conjugate analysis. We demonstrate that size shifts on the order of 1 nm are detectable, and that protein surface coverages (maximum number of proteins bound per unit surface area) can be inferred from measurements, with nanoparticle polydispersity considered.

EXPERIMENTAL SECTION

Materials and Sample Preparation. GNPs with nominal diameters of 20, 30, and 50 nm were purchased from Nanocomposix, Inc. (San Diego, USA). Electron microscopy revealed that these samples had mean diameters ± standard deviations of 18.6 ± 2.3 nm, 30.8 ± 3.3 nm, and 51.0 ± 5.7 nm, respectively. GNP surfaces were pretreated with tannic acid by the manufacturer to stabilize them in aqueous suspension. Bovine serum albumin (BSA) was purchased from Sigma-Aldrich (Saint Louis, MO, USA). BSA solutions were prepared by dispersing BSA powders in deionized (DI, obtained with a SpectraPure filtration system) water. GNPs suspensions, with manufacturer provided number concentrations (ranging from 3 × 10^9 to 8 × 10^{10} particles mL^{-1}), were mixed with known concentration BSA samples in a suspension volume of 1 mL in polypropylene centrifuge tubes. 5−7 GNP:BSA number concentration ratios (ranging from 1:3 to 1:12 000) were examined for each GNP size. Prior to measurements, samples were placed in an incubator (Alkali Scientific, FL, USA) at 38.0 °C for 16 h. Additionally, for 50 nm GNPs, incubation was also performed at 4 °C. No other sample preparation was required prior to LN-IMS measurement and nanoparticles were observed to remain stable in suspension during incubation. This is distinct from most studies utilizing charge reduction electrospray based aerosolization, where electrical conductivity modulation and analyte preconcentration are needed prior to analysis.

LN-IMS Measurements. The size distribution functions of bare GNPs and GNP-BSA conjugates were measured via a liquid nebulizer-ion mobility spectrometry (LN-IMS) system. Details of the operation of this system are provided in Jeon et al.[37] Briefly, in the LN employed (Model 9110, Kanomax FMT, St Paul, MN, USA), the GNP-BSA suspension at a sample flow rate of 0.01−1 mL min^{-1} is mixed with 100 mL min^{-1} of ultra-high-purity water (which contains total organic carbon and nonvolatile residues below 1 ppbv, was treated with 165 nm UV light, and was passed through 10 and 20 nm particle filtration systems as well as a mixed bed ion-exchange resin prior to system introduction). The ratio of the ultra-high-purity water flow rate to the sample flow rate defines the dilution factor for the measurement, which is adjustable from 10^2 to 10^4. The LN produces approximately log-normally distributed droplets with a geometric mean diameter of 99.8 nm and a geometric standard deviation of 2.32. Upon drying, aerosolized GNP:BSA conjugates were passed out of the LN using a flow of ultra-high-purity air, with neither fragmentation nor specific aggregation

DOI: 10.1021/acs.analchem.6b01555
Anal. Chem. XXXX, XXX, XXX−XXX

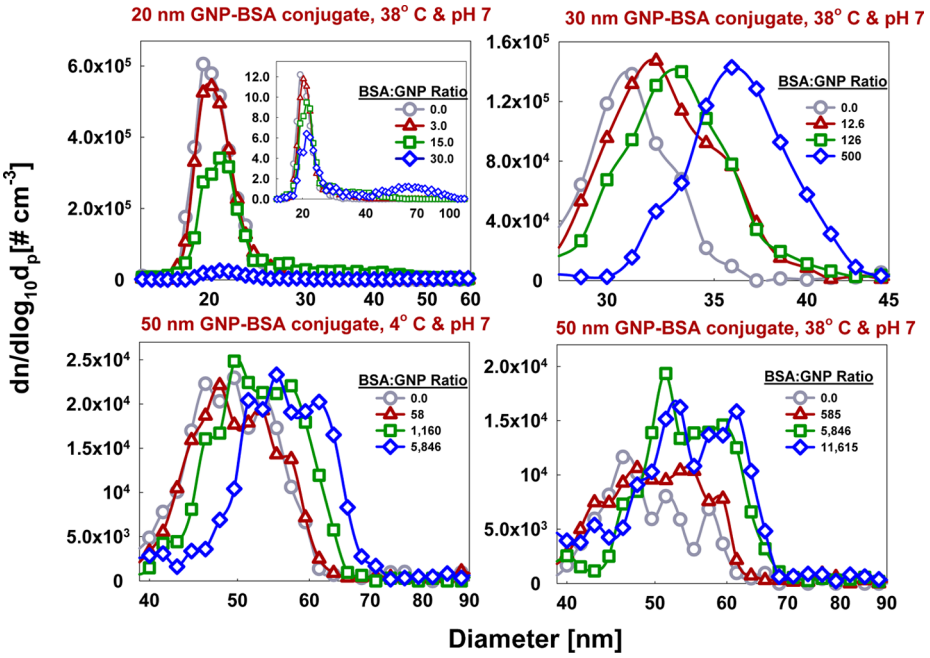

Figure 1. LN-IMS inferred size distribution functions (expressed as gas-phase number concentrations per unit $\log_{10}$ diameter, d n/d $\log_{10}d_p$) for GNP−BSA conjugates with varying BSA:GNP number concentration ratios in aqueous suspension. The upper left inset displays results for nominally 20 nm GNPs but with size distribution functions normalized by the total number concentration for each measurement.

caused by the aerosolization process. For IMS, the aerosolized conjugates were sent into a DMA (both models 3081 and 3085, TSI Inc., Shoreview MN, were applied in measurements)[39] followed by a butanol based condensation particle counter (CPC, model 3075, TSI Inc.). The DMA-CPC combination was operated as scanning mobility particle spectrometer (SMPS),[40] with 120 s scans applied and at least eight measured spectra per sample. Raw data consisted of CPC measured concentration as a function of mean voltage across the DMA electrodes. Using manufacturer provided software (Aerosol Instrument Manager), data were inverted to reveal the size distribution function, d n/d $\log_{10}(d_p)$, i.e., the aerosol particle number concentration per unit $\log_{10}$ diameter (with diameter in nanometers) as a function of diameter. Diameter was inferred using the Stokes-Millikan equation, found to be valid for nearly spherical particles in a variety of studies where air has been applied in IMS measurement.[41,42]

The dilution factor was varied 10^2 to 10^4 during measurements to optimize the signal-to-noise ratio as well as to mitigate nonspecific conjugate formation (which was predictable based on the nominal BSA concentration added). Lower dilution factors were applied to examine the size distribution functions of GNP−BSA conjugates, while higher dilution factors were applied to directly detect free BSA molecules in the suspension. As described in Jeon et al.,[37] individual BSA molecules themselves can be measured and quantified via LN-IMS, and using an LN-IMS specific calibration curve (relating the measured aerosol concentration to liquid suspension concentration) the size distribution function of the free BSA measured here was used to directly calculate the unbound BSA suspension concentration. The shifts in size distribution functions for GNP−BSA conjugates were examined as functions of unbound BSA concentration. We remark that the unbound BSA concentration was consistently found to be a factor of ∼2 lower than the nominal BSA number concentration, based on what was added to GNP:BSA suspensions. This is attributable to protein binding to the wall of the polypropylene vial used in incubation, an influence not considered in prior studies of GNP−BSA conjugation.

RESULTS AND DISCUSSION

Size Distribution Functions. After data inversion, which corrects for the transmission through the DMA,[43] the fraction of multiply charged particles examined,[44] and the depositional losses of particles in system tubing,[45] LN-IMS measurements lead to inference of the gas-phase size distribution function, which is specifically represented as the parameter d n/d $\log_{10}(d_p)$, i.e., the gas-phase number concentration per unit $\log_{10}$ particle diameter (in nanometers). Integration of d n/d $\log_{10}(d_p)$ across the entire diameter range yields the gas-phase number concentration of particles aerosolized by the LN-IMS. Size distribution functions (averaged over more than five spectra) of 20, 30, and 50 nm GNPs are displayed in Figure 1 for selected BSA:GNP number concentration ratios. Size distributions were corrected for the dilution factor employed in the LN (i.e., they were multiplied by the dilution factor); hence, the displayed values are proportional to the size distribution function in the original suspensions.[37] Error bars are not shown on plots, but we remark that because the error in IMS measurements scales with $N^{-1/2}$ (where N is the total number of particles counted for all samples) and more than 10^3 particles were measured for each data point, counting errors are ≤3% for nearly all data. Clearly evident for all samples except the nominally 20-nm-diameter GNPs is that with increasing BSA:GNP number concentration ratio, the peaks in size distributions corresponding to GNPs shift to the right. This is indicative of conjugate formation and an increased number of proteins bound at higher BSA concentration in suspension. However, distributions are noticeably broad relative to the extent of the shift, making difficult quantification of the extent of shift simply by comparing mode values in distributions (as has been common practice in prior studies[33]). This is most

DOI: 10.1021/acs.analchem.6b01555
Anal. Chem. XXXX, XXX, XXX−XXX

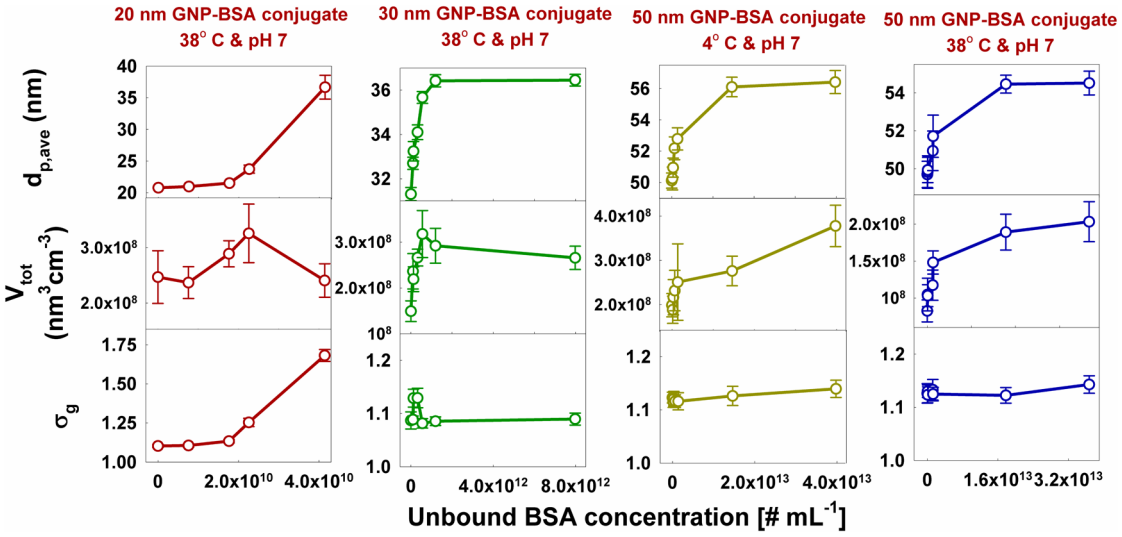

Figure 2. Summary of the mean diameter ($d_{p,ave}$), gas-phase volumetric concentration (V_{tot}), and geometric standard deviation (σ_g) as a function of the unbound BSA concentration in aqueous suspension.

problematic for the nominally 50 nm GNPs, where we observed oscillations in size distributions about peak values which are larger than the measurement error. These oscillations are present for all 50 nm samples (suggesting that the true distribution function is composed of several modes with mean diameters extremely close to one another, which has been found previously for commercial noble metal particles[35]), but are most apparent for the 38 °C GNP-BSA conjugates formed for BSA:GNP ratios of 5846 and 11 615. The perceived higher concentrations for these samples resulted from these measurements being taken on a different day than those for lower BSA:GNP ratios. The LN-IMS calibration for number concentration is known to vary by ±20% (but not for actually mobility, where calibration is relatively constant), as shown previously.[37] Shifts are less evident for nominally 20 nm GNPs; instead, we observed a decreasing number concentration near 20 nm and an increasing number concentration about 60 nm in LN-IMS measurements, with increasing BSA:GNP ratios.

To better quantify the extent of shift in size distribution functions, for each we calculate a mean diameter ($d_{p,ave}$), the conjugate volume concentration (V_{tot}), and a geometric standard deviation (σ_g), via the equations

$$d_{p,ave} = \frac{\int_{-\infty}^{\infty} \frac{dn}{d\log_{10} d_p} d_p d\log_{10} d_p}{\int_{-\infty}^{\infty} \frac{dn}{d\log_{10} d_p} d\log_{10} d_p} \quad (1a)$$

$$V_{tot} = \frac{\pi}{6} \int_{-\infty}^{\infty} \frac{dn}{d\log_{10} d_p} d_p^{\,3} d\log_{10} d_p \quad (1b)$$

$$\sigma_g = \exp\left(\sqrt{\frac{\int_{-\infty}^{\infty} \frac{dn}{d\log_{10} d_p} \ln^2\left(\frac{d_p}{d_{p,g}}\right) d\log_{10} d_p}{\int_{-\infty}^{\infty} \frac{dn}{d\log_{10} d_p} d\log_{10} d_p}} \right) \quad (1c)$$

$$d_{p,g} = \exp\left(\frac{\int_{-\infty}^{\infty} \frac{dn}{d\log_{10} d_p} \ln(d_p) d\log_{10} d_p}{\int_{-\infty}^{\infty} \frac{dn}{d\log_{10} d_p} d\log_{10} d_p} \right) \quad (1d)$$

In eq 1d, $d_{p,g}$ is the geometric mean diameter, which must be calculated to determine the geometric standard deviation. The geometric standard deviation quantifies the polydispersity of the size distribution, with $\sigma_g \leq 1.1$ typically regarded as monodisperse. Collectively, the noted parameters provide information on the growth of conjugates, as well as whether growth is due to BSA binding only or conjugate−conjugate binding (aggregation). The former would lead to modest increases in $d_{p,ave}$ and V_{tot}, and a decrease in σ_g (which would not be detectable for particles where σ_g is initially low). The latter would lead to a pronounced (tens of nanometers) increase in $d_{p,ave}$, but a more modest increase V_{tot} (V_{tot} only changes because of protein binding), and a σ_g in the range 1.3−1.4, irrespective of its initial value.[46]

Equations 1a−1d) are applicable to both polydisperse and multimodal distributions, which is important in the present study, particularly for the nominally 50-nm-diameter GNPs. Excluding the portion of each size distribution function attributed to isolated BSA, eqs 1a−1c) calculated parameters are plotted in Figure 2 as functions of unbound BSA concentration in suspensions. Error bars represent the standard deviation of each data point, evaluated by performing calculations for each measured size distribution function separately. Focusing first on the nominally 30 and 50 nm GNPs, we find for both samples that $d_{p,ave}$ increases rapidly at low BSA concentrations but appears to reach a maximum value as BSA concentration is further increased. Unlike alternative techniques, size shifts on the order of 1−2 nm are clearly detectable and larger than the measurement to measurement variability, despite the individual conjugate size distribution functions having standard deviations larger than 1−2 nm. This demonstrates directly that LN-IMS can be used to probe the earliest stages of conjugate formation, even for nanoparticles whose size distribution does not shift appreciably due to protein binding. Volume concentrations for these samples show similar behavior to $d_{p,ave}$ (increasing sharply with unbound BSA concentration at lower concentrations), and geometric standard deviations remain constant near 1.1 (indicating the samples are not perfectly monodisperse but remain narrowly distributed during measurements). For the nominally 50 nm GNPs, a larger extent of binding is observed at lower temperature.

DOI: 10.1021/acs.analchem.6b01555
Anal. Chem. XXXX, XXX, XXX−XXX

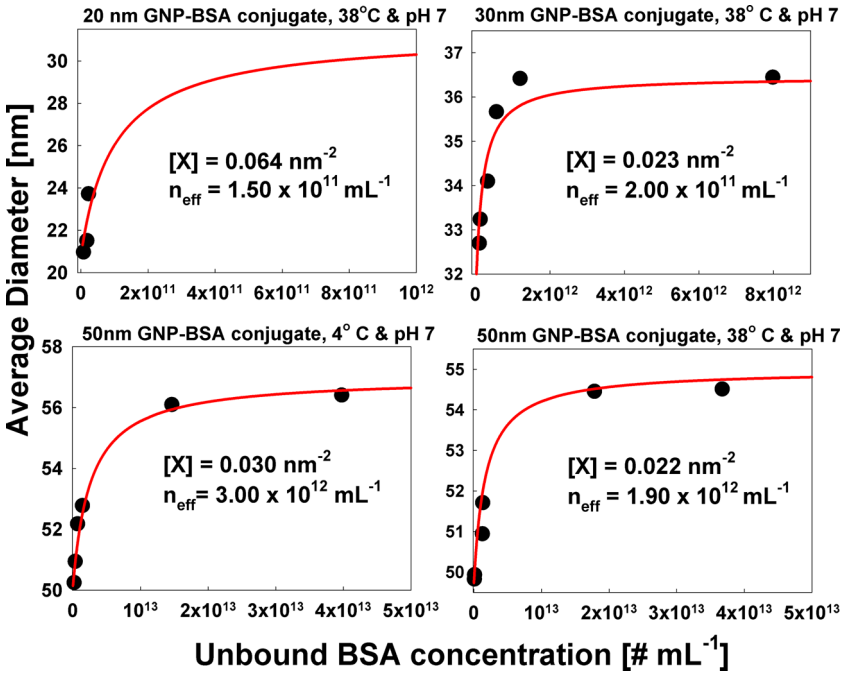

Figure 3. Measured (black circles) and calculated (red curves) average diameters of GNP−BSA conjugates as functions of the unbound BSA concentration. [X] refers to the site surface coverage parameter employed in the Langmuir-like sorption model, and correspondingly n_{eff} is the inferred protein concentration above a surface site.

Qualitatively, these measurements suggest that BSA binding to 30 and 50 nm GNPs does not drive conjugate−conjugate aggregation. Additionally, the near-constancy of $d_{p,ave}$ beyond a critical BSA concentration suggests that BSA binding is reversible (i.e., samples are equilibrated) and that GNPs can be saturated with BSA. Both of these findings are in line with the conclusions of prior studies of GNP−protein conjugation.[11,12,47] For 20 nm GNPs, unique behavior is observed; the $d_{p,ave}$ versus BSA concentration curve is concave upward, and the volume concentration stays relatively constant, and geometric standard deviation increases drastically (this was expected as samples became bimodal at increasing BSA concentration). We examine the mechanism of binding further in the subsequent section. In total, inverted size distribution functions and quantification of size distributions via eqs 1a−1c) reveal that LN-IMS is a viable approach to detect ∼1−2 nm shifts in nanoparticle size brought by conjugation with proteins, even in instances where the size distribution function varies by more than this amount.

Comparison with Binding and Aggregation Models. Poor size shift precision for nanoparticle−protein conjugates can limit the amount of information gained via measurements. For this reason, in studies utilizing DLS,[11] or in prior IMS studies in which only the mode diameter was examined,[30,33] only a maximum surface coverage of nanoparticles (expressed as the number of protein binding sites per unit nanoparticle surface area) has been inferred. For BSA binding onto gold, reported surface coverages near body temperature reported previously vary from study to study. Using a quartz crystal microbalance (QCM) Brewer et al.[47] reported a value of 0.037 nm^{-2} and Kaufman et al.[48] reported values ranging from 0.020 to 0.033 nm^{-2} for flat surfaces. Using IMS coupled with mass analysis, Guha et al.[30] determined a value of 0.027 nm^{-2} for nominally 30 nm, but in a previous study with IMS Tsai et al.[33] reported values of 0.023 nm^{-2}, 0.017 nm^{-2}, and 0.014 nm^{-2} for nominally 10, 30, and 60 nm GNPs, respectively. By examining precisely calculated mean diameters in inverted size distributions, here we show that not only can LN-IMS be used to infer surface coverages in line with QCM measurements, but also using a Langmuir-like binding model the effective protein concentration above a GNP surface (which defines how easily proteins dissociate from the surface) can be determined.

To develop a binding model which can be compared to measurements, first, we consider a nanoparticle with diameter $d_{p,0}$ in the absence of any conjugated protein. The nanoparticle has a binding site density of [X] sites per unit surface area, and above each site, the effective protein concentration is n_{eff} when a protein is bound. These two parameters determine the extent of conjugate binding for a given concentration of protein present in solution, and at equilibrium, the probability P_i this nanoparticle has i proteins bound to it is given as

$$P_0 = \frac{1.0}{1.0 + \sum_{k=1}^{k=[X]\pi d_{p,0}^2}\left[\left(\frac{n_a}{n_{eff}}\right)^k \prod_{j=1}^{j=k}\left(\frac{[[X]\pi d_{p,0}^2 - j + 1]}{j}\right)\right]} \quad (2a)$$

$$P_i = \frac{\left(\frac{n_a}{n_{eff}}\right)^i \prod_{j=1}^{i}\left(\frac{[[X]\pi d_{p,0}^2 - j + 1]}{j}\right)}{1.0 + \sum_{k=1}^{k=[X]\pi d_{p,0}^2}\left[\left(\frac{n_a}{n_{eff}}\right)^k \prod_{j=1}^{j=k}\left(\frac{[[X]\pi d_{p,0}^2 - j + 1]}{j}\right)\right]} \quad i \geq 1 \quad (2b)$$

where n_a is the concentration of unbound BSA in aqueous suspension. Equations 2a and 2b) are derived explicitly in the Supporting Information; the derivation follows a similar form to that used previously[49−51] to examine vapor molecule binding to ions in the gas phase. Using P_i to determine the fraction of particles with i proteins bound and considering the experimentally determined bare nanoparticle size distribution

DOI: 10.1021/acs.analchem.6b01555
Anal. Chem. XXXX, XXX, XXX−XXX

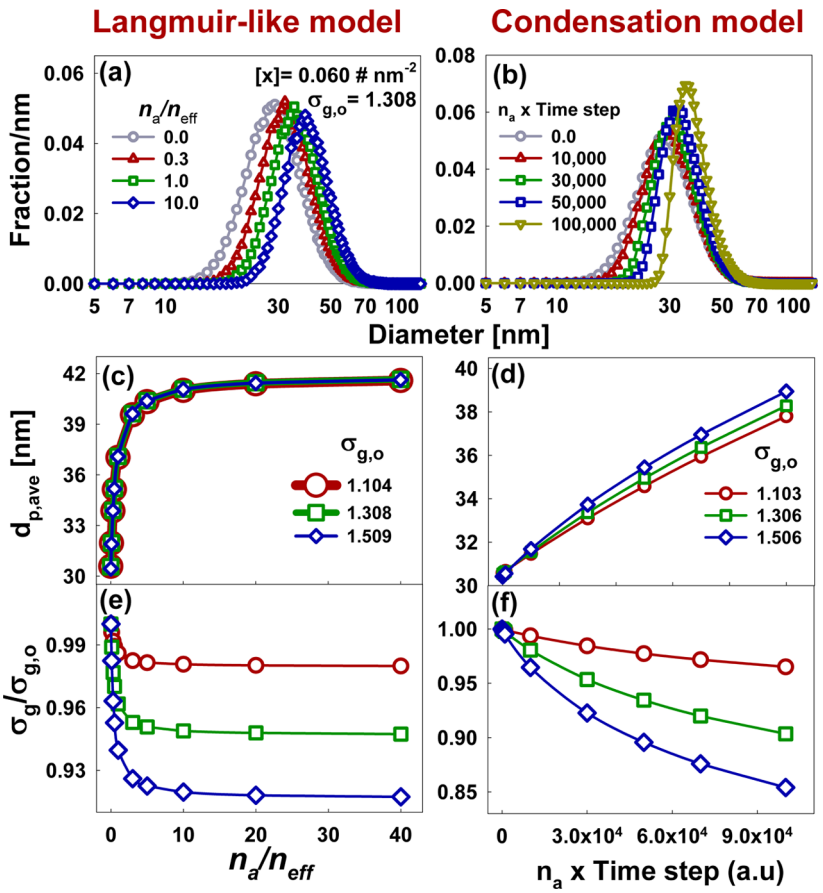

Figure 4. Normalized size distribution functions (a and b), mean diameters (c and d), and normalized geometric standard deviations (by the baseline value, e and f) of nanoparticle−protein conjugates as predicted by the Langmuir-like model (eq 2a) and an irreversible protein condensation model for log-normally distributed nanoparticles. Plots c−f are shown for variable initial geometric standard deviations.

function $\frac{dn}{d\log_{10} d_{p,0}}\rfloor_0$, the expected average diameter can then be calculated as

$$d_{p,ave} = \frac{\int_{-\infty}^{\infty} \frac{dn}{d\log_{10} d_{p,0}}\rfloor_0 \left(\sum_{i=0}^{\infty} d_{p,i} P_i\right) d\log_{10} d_{p,0}}{\int_{-\infty}^{\infty} \frac{dn}{d\log_{10} d_{p,0}}\rfloor_0 d\log_{10} d_{p,0}} \quad (3a)$$

where $d_{p,i}$ is a nanoparticle's effective mobility diameter with i protein molecules bound. Various models can be developed for $d_{p,i}$.[32,33] However, based on prior theoretical calculations[52] and mobility measurements of nonspherical aerosol particles,[36] we find that unless extremely nonspherical particles are expected to result from binding (for which there is no evidence), it is reasonable to approximate GNP:BSA conjugates as spherical, with mobility diameters equal to their volume equivalent diameters. Mobility diameters, $d_{p,i}$, are hence calculated as

$$d_{p,i} = (d_{p,0}^3 + i d_{pro}^3)^{1/3} \quad (3b)$$

where d_{pro} is the mobility diameter of a BSA monomer, measured to be 6.31 nm via IMS and in agreement with prior IMS[53,54] and ultracentrifugation measurements.[20] In applying eqs 2a and 2b and eq 3a in comparison to measurements, $[X]$ and n_{eff} are fitting parameters enabling prediction of $d_{p,ave}$ as a function of n_a. These equations can be applied to polydisperse and multimodal distributions; in applying them the main assumption is simply that $[X]$ and n_{eff} are not dependent on nanoparticle size. More detailed equilibrium binding models with size dependent parameters would result in altered equations for P_i, but eq 3a would remain unchanged.

Equation 3a predicted $d_{p,ave}$ values (taking measured distributions $\frac{dn}{d\log_{10} d_{p,0}}\rfloor_0$ and concentrations n_a as inputs) are plotted in comparison to experimentally inferred values in Figure 3. For nominally 20 nm gold nanospheres, only three data points were used, as the appearance of a second mode near 60 nm cannot be explained via the Langmuir-like equilibrium binding model alone. Binding model parameters inferred for these nanoparticles are thus only shown for completeness and are not utilized in comparison to prior results. For the 30 and 50 nm GNPs (at both 4 and 37 °C), the two parameter model can be fit extremely well to measurements, and the resulting surface coverage values, ranging from 0.022 to 0.030 nm^{-2}, are in excellent agreement with the previous QCM measurements and the IMS-mass measurements of Guha et al.[30] This further confirms the applicability of LN-IMS analysis to examine nanoparticle−protein conjugates, and suggests that in electrospray based aerosolization studies,[33] mode mobility diameter measurements of nanoparticles may be skewed by the presence of nonvolatile residue, which would directly influence inferred surface coverage values. Interestingly, the effective surface concentrations of proteins (which are linked directly to the dissociation constant of proteins from conjugates) are found to decrease by almost an order of magnitude as GNP nominal diameter decreases from 50 to 30 nm. This suggests that with increasing surface curvature, BSA is adsorbed with increasing

DOI: 10.1021/acs.analchem.6b01555
Anal. Chem. XXXX, XXX, XXX−XXX

affinity to GNP. This is also supported by the appearance of a larger mode in nominally 20 nm distributions, which is presumably brought about by conjugate−conjugate aggregation. Though nanoparticle size dependencies on conjugate formation have been examined previously,[55,56] this specific finding appears to be new, and size dependencies in the strength of nanoparticle−protein bounds will need to be examined in future work.

Though the comparison presented in Figure 3 suggests that at equilibrium, the Langmuir-like binding model (eq 2a) satisfactorily describes LN-IMS measurements, it is important to compare results to alternative models. One possibility is the irreversible condensation of proteins on nanoparticles, forming continuously growing conjugates at a rate limited by the diffusion limited aggregation rate of proteins onto nanoparticles/conjugates.[57] To compare such a condensation model to measurements, we perform a constant number of Monte Carlo simulations[58] to predict the evolution of the size distribution functions of protein−nanoparticle conjugates formed via irreversible, diffusion limited protein condensation. Details on simulations on are provided in the Supporting Information, and results are directly compared to the aforementioned Langmuir-like binding model in Figure 4. Specifically, for log-normally distributed nanoparticles with a geometric mean diameter of 30 nm and geometric standard deviations near 1.1, 1.3, and 1.5 (near monodisperse to highly polydisperse), the normalized size distribution functions (fraction of particles per nm), mean nanoparticle−conjugate diameter, and geometric standard deviation are plotted as functions of the suspension protein concentration (n_a) to effective protein concentration (n_{eff}) ratio for the Langmuir-like model, and the product of suspension protein concentration and simulation time step for the condensation model. The abscissa for the condensation model results is labeled as such, because in irreversible condensation, proteins would continuously bind to BSA, i.e., a maximum surface coverage does not exist, and the size distribution would continuously vary over time. Nonetheless, as the abscissas on all plots are directly proportional to protein concentration in suspension, results are qualitatively comparable to one another. It is apparent that the condensation model predicts a steady increase in the mean nanoparticle−protein conjugate diameter as well as a steady decrease in the geometric standard deviation for all samples with continued binding; neither is observed in measurements, further suggesting that nanoparticle−protein binding is a reversible process best described by a Langmuir-like binding model. Additionally, the condensation-like model is not in qualitative agreement with the changes in the size distribution function observed for nominally 20 nm GNPs, suggesting that a more detailed aggregation model, considering conjugate−conjugate binding, is needed for this sample.

CONCLUSIONS

Electrospray ionization and electrospray based aerosolization techniques have arguably been the most important developments in biomolecular and macromolecular analysis in the past several decades, enabling mass spectrometry, and more recently, ion mobility spectrometry of biomolecular complexes.[59] However, despite initial success in analyzing nanoparticle−protein complexes through electrospray based aerosolization,[30,33,60] the intrinsic requirements of electrospray solutions, including proper electrical conductivity and low nonvolatile solute content, are simply incompatible with the suspension requirements for many nanoparticle−protein conjugate analyses (i.e., nonvolatile solutes required for nanoparticle stability and/or high salt content to mimic biological conditions). Here, we have demonstrated that liquid nebulization with online ultra-high-purity water dilution can be used in lieu of electrospray to aerosolize nanoparticle−protein conjugates, facilitating their examination via ion mobility spectrometry. We further show that, via integrating across complete size distribution functions inferred in IMS measurement, relatively polydisperse samples can be examined, as a shift in mobility equivalent size on the order of 1−2 nm can be examined. Surface coverage parameters inferred from LN-IMS measurements are further shown to be in excellent agreement with parameters inferred from quartz crystal microbalance measurements. Moving forward, we suggest that LN-IMS measurements are a viable alternative to dynamic light scattering, and as prior work has shown that LN-IMS measurements can be made in higher salt concentration suspensions,[37] LN-IMS analysis will find utility as a method to study nanoparticle−protein conjugate formation. Future coupling of LN-IMS with aerosol particle mass analysis[30] and/or inductively coupled plasma mass spectrometry[61] should also enable more detailed characterization of nanoparticle−protein conjugates.

ASSOCIATED CONTENT

Supporting Information

The Supporting Information is available free of charge on the ACS Publications website at DOI: 10.1021/acs.analchem.6b01555.

Derivation of the Langmuir-like binding model employed, as well as the constant number Monte Carlo simulations employed in comparison to measurements (PDF)

AUTHOR INFORMATION

Corresponding Author

*E-mail: hogan108@ umn.edu. Tel: 1-612-626-8312. Fax: 1-612-625-6069.

Notes

The authors declare the following competing financial interest(s): D. R. Oberreit is an employee of Kanomax-FMT; Kanomax-FMT manufactures the liquid nebulization system utilized in measurements (Model 9110). The remaining authors declare no competing financial interests.

ACKNOWLEDGMENTS

Preliminary studies associated with this work were supported by National Science Foundation Award CBET-1133285. S. Jeon was supported by United States Army Research Office Award MURI W911NF-12-0407.

REFERENCES

(1) Ashby, J.; Duan, Y. K.; Ligans, E.; Tamsi, M.; Zhong, W. W. *Anal. Chem.* **2015**, *87*, 2213−2219.
(2) Ashby, J.; Schachermeyer, S.; Pan, S. Q.; Zhong, W. W. *Anal. Chem.* **2013**, *85*, 7494−7501.
(3) Maiolo, D.; Bergese, P.; Mahon, E.; Dawson, K. A.; Monopoli, M. P. *Anal. Chem.* **2014**, *86*, 12055−12063.
(4) Mudalige, T. K.; Qu, H. O.; Linder, S. W. *Anal. Chem.* **2015**, *87*, 7395−7401.

DOI: 10.1021/acs.analchem.6b01555
Anal. Chem. XXXX, XXX, XXX−XXX

(5) Cedervall, T.; Lynch, I.; Lindman, S.; Berggard, T.; Thulin, E.; Nilsson, H.; Dawson, K. A.; Linse, S. *Proc. Natl. Acad. Sci. U. S. A.* **2007**, *104*, 2050−2055.
(6) Liu, R.; Jiang, W.; Walkey, C. D.; Chan, W. C. W.; Cohen, Y. *Nanoscale* **2015**, *7*, 9664−9675.
(7) Sykes, E. A.; Chen, J.; Zheng, G.; Chan, W. C. W. *ACS Nano* **2014**, *8*, 5696−5706.
(8) Walkey, C. D.; Chan, W. C. W. *Chem. Soc. Rev.* **2012**, *41*, 2780−2799.
(9) Walkey, C. D.; Olsen, J. B.; Song, F. Y.; Liu, R.; Guo, H. B.; Olsen, D. W. H.; Cohen, Y.; Emili, A.; Chan, W. C. W. *ACS Nano* **2014**, *8*, 2439−2455.
(10) Dobrovolskaia, M. A.; Patri, A. K.; Zheng, J.; Clogston, J. D.; Ayub, N.; Aggarwal, P.; Neun, B. W.; Hall, J. B.; McNeil, S. E. *Nanomedicine* **2009**, *5*, 106−117.
(11) Jans, H.; Liu, X.; Austin, L.; Maes, G.; Huo, Q. *Anal. Chem.* **2009**, *81*, 9425−9432.
(12) Dominguez-Medina, S.; Blankenburg, J.; Olson, J.; Landes, C. F.; Link, S. *ACS Sustainable Chem. Eng.* **2013**, *1*, 833−842.
(13) Calzolai, L.; Franchini, F.; Gilliland, D.; Rossi, F. *Nano Lett.* **2010**, *10*, 3101−3105.
(14) Montes-Burgos, I.; Walczyk, D.; Hole, P.; Smith, J.; Lynch, I.; Dawson, K. *J. Nanopart. Res.* **2010**, *12*, 47−53.
(15) Filipe, V.; Hawe, A.; Jiskoot, W. *Pharm. Res.* **2010**, *27*, 796−810.
(16) James, A. E.; Driskell, J. D. *Analyst* **2013**, *138*, 1212−1218.
(17) Chen, A. L.; Hu, Y. S.; Jackson, M. A.; Lin, A. Y.; Young, J. K.; Langsner, R. J.; Drezek, R. A. *Nanoscale Res. Lett.* **2014**, *9*.
(18) Zijlstra, P.; Paulo, P. M. R.; Orrit, M. *Nat. Nanotechnol.* **2012**, *7*, 379−382.
(19) Walter, J.; Thajudeen, T.; Süβ, S.; Segets, D.; Peukert, W. *Nanoscale* **2015**, *7*, 6574−6587.
(20) Walter, J.; Lohr, K.; Karabudak, E.; Reis, W.; Mikhael, J.; Peukert, W.; Wohlleben, W.; Colfen, H. *ACS Nano* **2014**, *8*, 8871−8886.
(21) Bohrer, B. C.; Merenbloom, S. I.; Koeniger, S. L.; Hilderbrand, A. E.; Clemmer, D. E. *Annu. Rev. Anal. Chem.* **2008**, *1*, 293−327.
(22) Bacher, G.; Szymanski, W. W.; Kaufman, S. L.; Zollner, P.; Blaas, D.; Allmaier, G. *J. Mass Spectrom.* **2001**, *36*, 1038−1052.
(23) Fernandez de la Mora, J.; de Juan, L.; Eichler, T.; Rosell, J. *TrAC, Trends Anal. Chem.* **1998**, *17*, 328−339.
(24) Kaufman, S. L.; Skogen, J. W.; Dorman, F. D.; Zarrin, F.; Lewis, K. C. *Anal. Chem.* **1996**, *68*, 1895−1904.
(25) Stolzenburg, M. R.; Mcmurry, P. H. *Aerosol Sci. Technol.* **1991**, *14*, 48−65.
(26) Wiedensohler, A.; Birmili, W.; Nowak, A.; Sonntag, A.; Weinhold, K.; Merkel, M.; Wehner, B.; Tuch, T.; Pfeifer, S.; Fiebig, M.; Fjaraa, A. M.; Asmi, E.; Sellegri, K.; Depuy, R.; Venzac, H.; Villani, P.; Laj, P.; Aalto, P.; Ogren, J. A.; Swietlicki, E.; Williams, P.; Roldin, P.; Quincey, P.; Huglin, C.; Fierz-Schmidhauser, R.; Gysel, M.; Weingartner, E.; Riccobono, F.; Santos, S.; Gruning, C.; Faloon, K.; Beddows, D.; Harrison, R. M.; Monahan, C.; Jennings, S. G.; O'Dowd, C. D.; Marinoni, A.; Horn, H. G.; Keck, L.; Jiang, J.; Scheckman, J.; McMurry, P. H.; Deng, Z.; Zhao, C. S.; Moerman, M.; Henzing, B.; de Leeuw, G.; Loschau, G.; Bastian, S. *Atmos. Meas. Tech.* **2012**, *5*, 657−685.
(27) Dudkiewicz, A.; Wagner, S.; Lehner, A.; Chaudhry, Q.; Pietravalle, S.; Tiede, K.; Boxall, A. B. A.; Allmaier, G.; Tiede, D.; Grombe, R.; von der Kammer, F.; Hofmann, T.; Molhave, K. *Analyst* **2015**, *140*, 5257−5267.
(28) Tsai, D. H.; Zangmeister, R. A.; Pease, L. F., III; Tarlov, M. J.; Zachariah, M. R. *Langmuir* **2008**, *24*, 8483−8490.
(29) Scalf, M.; Westphall, M. S.; Krause, J.; Kaufman, S. L.; Smith, L. M. *Science* **1999**, *283*, 194−197.
(30) Guha, S.; Ma, X.; Tarlov, M. J.; Zachariah, M. R. *Anal. Chem.* **2012**, *84*, 6308−6311.
(31) Li, M.; Guha, S.; Zangmeister, R. A.; Tarlov, M. J.; Zachariah, M. R. *Aerosol Sci. Technol.* **2011**, *45*, 849−860.
(32) Pease, L. F.; Tsai, D. H.; Zangmeister, R. A.; Zachariah, M. R.; Tarlov, M. J. *J. Phys. Chem. C* **2007**, *111*, 17155−17157.
(33) Tsai, D. H.; DelRio, F. W.; Keene, A. M.; Tyner, K. M.; MacCuspie, R. I.; Cho, T. J.; Zachariah, M. R.; Hackley, V. A. *Langmuir* **2011**, *27*, 2464−2477.
(34) Tsai, D. H.; DelRio, F. W.; MacCuspie, R. I.; Cho, T. J.; Zachariah, M. R.; Hackley, V. A. *Langmuir* **2010**, *26*, 10325−10333.
(35) Lenggoro, I. W.; Widiyandari, H.; Hogan, C. J.; Biswas, P.; Okuyama, K. *Anal. Chim. Acta* **2007**, *585*, 193−201.
(36) Gopalakrishnan, R.; McMurry, P. H.; Hogan, C. J. *J. Aerosol Sci.* **2015**, *82*, 24−39.
(37) Jeon, S.; Oberreit, D. R.; Van Schooneveld, G.; Hogan, C. J. *Analyst* **2016**, *141*, 1363−1375.
(38) Fissan, H.; Ristig, S.; Kaminski, H.; Asbach, C.; Epple, M. *Anal. Methods* **2014**, *6*, 7324−7334.
(39) Chen, D. R.; Pui, D. Y. H.; Hummes, D.; Fissan, H.; Quant, F. R.; Sem, G. J. *J. Aerosol Sci.* **1998**, *29*, 497−509.
(40) Wang, S. C.; Flagan, R. C. *Aerosol Sci. Technol.* **1990**, *13*, 230−240.
(41) Larriba, C.; Hogan, C. J.; Attoui, M.; Borrajo, R.; Fernandez-Garcia, J.; Fernandez de la Mora, J. *Aerosol Sci. Technol.* **2011**, *45*, 453−467.
(42) Kim, J. H.; Mulholland, G. W.; Kukuck, S. R.; Pui, D. Y. H. *J. Res. Natl. Inst. Stand. Technol.* **2005**, *110*, 31−54.
(43) Stolzenburg, M. R.; McMurry, P. H. *Aerosol Sci. Technol.* **2008**, *42*, 421−432.
(44) Gopalakrishnan, R.; McMurry, P. H.; Hogan, C. J. *Aerosol Sci. Technol.* **2015**, *49*, 1181−1194.
(45) Gormley, P. G.; Kennedy, M. *Proceedings of the Irish Royal Academy* **1949**, *52A*, 163−169.
(46) Vemury, S.; Pratsinis, S. E. *J. Aerosol Sci.* **1995**, *26*, 175−185.
(47) Brewer, S. H.; Glomm, W. R.; Johnson, M. C.; Knag, M. K.; Franzen, S. *Langmuir* **2005**, *21*, 9303−9307.
(48) Kaufman, E. D.; Belyea, J.; Johnson, M. C.; Nicholson, Z. M.; Ricks, J. L.; Shah, P. K.; Bayless, M.; Pettersson, T.; Feldotö, Z.; Blomberg, E.; Claesson, P.; Franzen, S. *Langmuir* **2007**, *23*, 6053−6062.
(49) Oberreit, D.; Rawat, V. K.; Larriba-Andaluz, C.; Ouyang, H.; McMurry, P. H.; Hogan, C. J. *J. Chem. Phys.* **2015**, *143*, 104204.
(50) Oberreit, D. R.; McMurry, P. H.; Hogan, C. J. *Phys. Chem. Chem. Phys.* **2014**, *16*, 6968−6979.
(51) Rawat, V. K.; Vidal-de-Miguel, G.; Hogan, C. J. *Analyst* **2015**, *140*, 6945−6954.
(52) Zhang, C.; Thajudeen, T.; Larriba, C.; Schwartzentruber, T. E.; Hogan, C. J. *Aerosol Sci. Technol.* **2012**, *46*, 1065−1078.
(53) Bush, M. F.; Hall, Z.; Giles, K.; Hoyes, J.; Robinson, C. V.; Ruotolo, B. T. *Anal. Chem.* **2010**, *82*, 9557−9565.
(54) Maisser, A.; Premnath, V.; Ghosh, A.; Nguyen, T. A.; Attoui, M.; Hogan, C. J. *Phys. Chem. Chem. Phys.* **2011**, *13*, 21630−21641.
(55) Lacerda, S. H. D. P.; Park, J. J.; Meuse, C.; Pristinski, D.; Becker, M. L.; Karim, A.; Douglas, J. F. *ACS Nano* **2010**, *4*, 365−379.
(56) Teichroeb, J. H.; Forrest, J. A.; Jones, L. W. *Eur. Phys. J. E: Soft Matter Biol. Phys.* **2008**, *26*, 411−415.
(57) Northrup, S. H.; Allison, S. A.; McCammon, J. A. *J. Chem. Phys.* **1984**, *80*, 1517−1526.
(58) Smith, M.; Matsoukas, T. *Chem. Eng. Sci.* **1998**, *53*, 1777−1786.
(59) Ruotolo, B. T.; Benesch, J. L. P.; Sandercock, A. M.; Hyung, S. J.; Robinson, C. V. *Nat. Protoc.* **2008**, *3*, 1139−1152.
(60) Tsai, D. H.; DelRio, F. W.; Pettibone, J. M.; Lin, P. A.; Tan, J. J.; Zachariah, M. R.; Hackley, V. A. *Langmuir* **2013**, *29*, 11267−11274.
(61) Elzey, S.; Tsai, D.-H.; Yu, L. L.; Winchester, M. R.; Kelley, M. E.; Hackley, V. A. *Anal. Bioanal. Chem.* **2013**, *405*, 2279−2288.

DOI: 10.1021/acs.analchem.6b01555
Anal. Chem. XXXX, XXX, XXX−XXX